Modeling sandwave formation in a numerical shallow water model

BORSJE Bas W.
Water Engineering & Managements, University of Twente, Enschede, The Netherlands
Marine and Coastal Systems, Deltares, Delft, The Netherlands

ROOS Pieter C.
Water Engineering & Management, University of Twente, Enschede, The Netherlands

KRANENBURG Wouter M.
Water Engineering & Management, University of Twente, Enschede, The Netherlands

HULSCHER Suzanne J.M.H.
Water Engineering & Management, University of Twente, Enschede, The Netherlands

ABSTRACT: Tidal sandwaves are prominent dynamic bottom features in shallow sandy seas such as the southern North Sea. Up to now, the processes controlling the dynamics of these bedforms have only been studied in idealized models, which assume schematized geometry, boundary conditions and turbulence models. Alternatively, in this paper we present simulations of sandwave formation with a numerical shallow water model (Delft3D). Reproduction of the basic sandwave formation mechanisms in a numerical shallow water model requires careful treatment of model geometry, initial profile, vertical resolution and lateral boundary conditions. Next, we compare results for two of the built-in turbulence models: the constant eddy viscosity model (commonly used in idealized models) and k-ε turbulence model. Finally, the outcome of the model is compared with field data on sandwave length, showing good agreement for the k-ε turbulence model.

1 INTRODUCTION

Large parts of the sandy seabed of shallow seas, such as the North Sea, are covered with rhythmic bed patterns. These bed patterns are the result of the complex interaction between hydrodynamics, sediment transport and morphology. The most dynamic large scale bed patterns are tidal sandwaves, which regenerate in several years time (Knaapen and Hulscher, 2002), may grow up to 25% of the water depth (McCave, 1971), have wavelengths (distance between two successive crests) in the order of hundreds of meters (Van Dijk and Kleinhans, 2005) and migrate at a speed up to tens of metres per year (Dorst et al., 2009). In the Southern North Sea, sandwaves are observed in water depths in the order of 25 m, flow velocities around 0.65 m s^{-1} and median grain sizes of 0.35 mm (Borsje et al., 2009).
Given their dynamic behavior, sandwaves may pose a hazard to offshore activities, by reducing the water depth of navigation channels, exposing pipelines and telecommunication cables and scouring offshore platforms or wind turbines (Németh et al., 2003). Consequently, insight in the processes controlling the variation in tidal sandwave length is essential for cost effective management practices.
Hulscher (1996) showed that sandwave formation can be explained as an inherent instability of the sandy seabed subject to tidal motion. The interaction of the oscillatory tidal current with a bottom perturbation gives rise to a tide-averaged residual circulation directed from the trough towards the crest of the sandwave. This residual circulation induces a net sediment flux towards the crest of sandwaves, which lead to sandwave growth if it overcomes the opposite effect of gravity. The model by Hulscher (1996) describes the hydrodynamics by using the three-dimensional shallow water equations. The turbulent stresses are

accounted for by combining a constant eddy viscosity with a partial slip condition at the bed and sediment transport is only modeled as bedload. Despite the strongly schematized representation of the physical processes, the occurrence of sandwaves in the Southern North Sea was predicted reasonably (Hulscher and van den Brink, 2001). Next, Németh et al. (2002) and Besio et al. (2004) introduced the effect of a residual current and tidal asymmetry respectively, which induce sandwave migration. In both models a constant eddy viscosity in combination with a partial slip condition at the bed is adopted. Besio et al. (2006) extended the model proposed by Hulscher (1996) by introducing a depth dependent eddy viscosity in combination with a no-slip condition at the bed. Moreover, both bedload and suspended load are included in the model. Comparison of the model outcome with field data showed that the model was able to reproduce the sandwave length at different locations on the Belgium Continental Shelf fairly well (Cherlet et al., 2007).
All the models discussed above are based on a linear stability analysis. In a linear stability analysis the growth rate of different perturbations is determined and the perturbation with the fastest growing mode is assumed to prevail. A consequence of this method is that the model validity is limited to small-amplitude sandwaves. Therefore, Németh et al. (2007) and Sterlini et al. (2009) proposed a non-linear model in which the sandwave behavior is modeled from its initial stage till its finite amplitude. In both models a constant eddy viscosity in combination with a partial slip condition at the bed is adopted.
In this paper we explore the possibility to study sandwave formation in a numerical shallow water model. The advantage of such a model approach is that many physical processes can be included in a sophisticated way (e.g. wind- and wave-driven currents, density gradients, sediment transport, complex turbulence models). However, given the high spatial and temporal resolution needed to model the growth of sandwaves, these type of models require large computational effort. Also, treatment of lateral boundary conditions requires care. The only study in which a numerical shallow model was used to investigate morphodynamic behavior of a sandwave was done by Tonnon et al. (2007). However, their study focused on one artificial sandwave, which makes it difficult to understand the processes controlling the formation of natural sandwaves. In this study, we use the numerical shallow water model Delft3D with a schematized geometry and only bedload sediment transport to study sandwave formation.
The main aim of this paper is to reproduce sandwave formation with a numerical shallow water model. Next to that we aim to compare two of the built-in turbulence models: constant eddy viscosity and k-ε and the effect on sandwave formation. Finally, we aim to compare model results with field measurements on sandwave length.
The outline of this paper is as follows. First, the Delft3D model setup is outlined, including model equations, boundary conditions and geometry (Section 2). Next, model results are presented with specific attention for the residual circulation and the growth rates. Next, the impact of the k-ε turbulence model on sandwave formation is compared with the constant eddy viscosity model (Section 3.1-3.2). The model outcome is compared with sandwave lengths as observed in the Southern North Sea (Section 3.3). Section 4 discusses the main findings of this paper, focusing on the similarities and differences between idealized models and the Delft3D model. Finally, important general conclusions are given (Section 5).

2 MODEL DESCRIPTION

2.1 Hydrodynamics

The formation of sandwaves is modeled using the numerical shallow water model Delft3D-FLOW (Lesser et al., 2004). The system of equations consists of the horizontal momentum equations, a continuity equation, a turbulence closure model, a sediment transport equation and a sediment continuity equation. The vertical momentum equation is reduced to the hydrostatic pressure relation as vertical accelerations are assumed to be small compared to gravitational acceleration. The model equations are solved by applying sigma layering in the vertical. In this study, the model is run in the 2DV mode, i.e. considering flow and variation in *x* and *z* direction only, while assuming zero flow and uniformity in *y* direction.
The 2DV hydrostatic shallow water equations are described by:

$$\frac{\partial u}{\partial t}+u\frac{\partial u}{\partial x}+\frac{\omega}{H+\zeta}\frac{\partial u}{\partial \sigma}=-\frac{1}{\rho_w}P_u+F_u+\frac{1}{\left(H+\zeta\right)^2}\frac{\partial}{\partial \sigma}\left(\upsilon_v\frac{\partial u}{\partial \sigma}\right), \qquad (1)$$

$$\frac{\partial \omega}{\partial \sigma} = -\frac{\partial \zeta}{\partial t} - \frac{\partial \left[(H+\zeta) u \right]}{\partial x}, \tag{2}$$

where u is the horizontal velocity, ω is vertical velocity relative to the moving vertical σ-plane, ρ_w is the water density, H water depth below reference datum, $d = H + \zeta$ the total water depth, P_u the pressure gradient, F_u the horizontal viscosity and v_V the vertical eddy viscosity.
Two different turbulence models are used in the simulations presented in this paper. The first turbulence model (Equation 3-I) is a constant value for the vertical eddy viscosity v_V both in time and space (Fredsøe and Deigaard, 1992). The second turbulence model (Equation 3-II) is the more advanced k-ε turbulence closure model in which both the turbulent energy k and the dissipation ε are computed (Rodi, 1984). The resulting vertical eddy viscosity v_V is variable both in time and space

$$\text{(I)} \quad \upsilon_v = \frac{\kappa U H_0 \sqrt{g}}{6C} \quad , \quad \text{(II)} \quad \upsilon_v = c_\mu \frac{k^2}{\varepsilon}, \tag{3}$$

in which κ is the von kármán constant, U is the amplitude of the depth averaged flow velocity, H_0 is the mean water depth, g is the gravitational acceleration, C is the Chézy roughness coefficient and c_μ is a constant with a recommended value of 0.09 (Rodi, 1984).
At the bed, a quadratic friction law is applied and the vertical velocity ω is set to zero at the bed

$$\tau_b \equiv \rho_w \frac{\upsilon_V}{d} \frac{\partial u}{\partial \sigma} = \rho_w u_* |u_*| \quad , \quad \omega = 0 \ \text{ at } \sigma = -1, \tag{4}$$

in which τ_b is the bed shear stress and u_* is the shear velocity, that relates the velocity gradient at the bed to the velocity u in the lowest computational grid point by assuming a logarithmic velocity profile.
At the free surface, a no-stress condition is applied and the vertical velocity ω is set to zero

$$\rho_w \frac{\upsilon_V}{d} \frac{\partial u}{\partial \sigma} = 0 \quad , \quad \omega = 0 \ \text{ at } \sigma = 0. \tag{5}$$

At the lateral boundaries, a so-called Riemann boundary condition is imposed (Verboom and Slob, 1984). For this type of boundary condition, outgoing waves are allowed to cross the open boundary without being reflected back into the computational domain, as happens for other type of boundary conditions.

2.2 Sediment transport and bed evolution

The bed load sediment transport, S_b is calculated by (Van Rijn et al., 2004)

$$|S_b| = 0.006 \alpha_s \rho_s w_s d_{50} M^{0.5} M_e^{0.7}, \tag{6}$$

where α_s is a correction parameter for the slope effects (see below), ρ_s is the specific density of the sediment, w_s is the settling velocity of the sediment and d_{50} the median sediment diameter. M and M_e, the sediment mobility number and excess sediment mobility number, respectively, are

$$M = \frac{v_r^2}{(s-1) g d_{50}} \quad , \quad M_e = \frac{(v_r - v_{cr})^2}{(s-1) g d_{50}}, \tag{7}$$

where v_r is the magnitude of an equivalent depth-averaged velocity computed from the velocity in the bottom computational layer assuming a logarithmic velocity profile, v_{cr} is the critical depth-averaged velocity for the initiation of motion based on the Shields curve and s is the relative density (ρ_s/ρ_w).
Bed load transport is affected by bed level gradients, which makes sediment transported downhill more easily than uphill. The correction parameter for the slope effect is (Bagnold, 1956):

$$\alpha_s = \lambda_s \left[\frac{\tan\phi}{\cos\left(\tan^{-1}\beta\right)\left(\tan\phi - \beta\right)} - 1 \right], \tag{8}$$

where λ_s is a user-defined slope parameter, β is the slope of the bed and φ the angle of internal fraction (angle of repose).
Finally, the bed evolution is governed by the sediment continuity equation (Exner equation), which reads

$$\left(1-\varepsilon_p\right)\frac{\partial z_b}{\partial t} + \frac{\partial S_b}{\partial x} = 0, \tag{9}$$

in which ε_p is the bed porosity. Relation (9) simply states that convergence (or divergence) of the sediment flux must be accompanied by a rise (or fall) of the bed profile.

2.3 Model set-up

In the horizontal, the model domain is divided in 558 grid cells, with a variable horizontal resolution. In the centre of the model domain the grid size is 10 meters, increasing to a value of 1500 m at the lateral boundaries. In the vertical, the model grid is divided in 20 layers, with small vertical resolution near the bed and increasing vertical resolution towards the water surface. At the lateral boundaries a depth-averaged velocity amplitude U of 0.65 m/s and a tidal period T of 12 hours is imposed. The initial bed level is prescribed by a multiplication of a sinusoidal sandwave pattern of a given wavelength with an envelope function (Figure 1), ensuring a gradual transition from the flat bed towards the sandwave field. Consequently, a coarser grid can be used near the boundaries. The mean water depth H_0 = 25 m and the median grain size d = 0.35 mm. The bed roughness C = 65 $m^{1/2}/s$ and the slope parameter λ_s = 2.5 (both parameters default Delft3D setting (Deltares, 2011)). The initial amplitude of the sandwave A_0 is 2% of the water depth. The model is run for two tidal cycles. The first tidal cycle is used for spin-up and no bed level changes are computed during this period. The second tidal cycle is used for determining the bed level evolution.

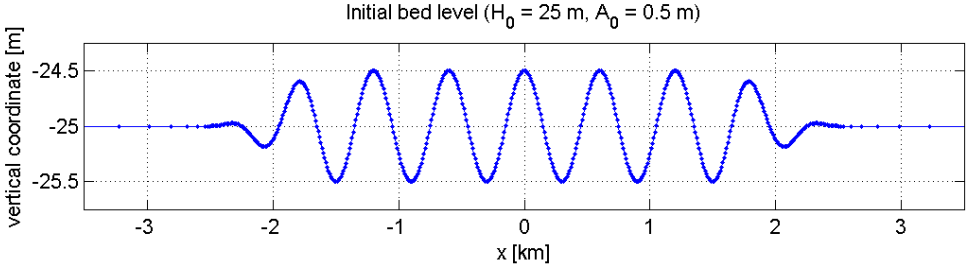

Figure 1. Initial bed level with, in this case, wavelength L = 600 m and initial amplitude A_0 = 0.5 m. The crest of the central sandwave is located at x = 0.

3 MODEL RESULTS

3.1 Hydrodynamics

First, we study the effect of the wavy bed on the flow velocity. Focusing on the position halfway the slope of the central sandwave (x = -L/4), the absolute maximum flow velocity near the bed is higher during flood, compared tot the absolute maximum flow velocity during ebb. Averaged over one tidal cycle, the flow velocity profiles show a circulation cell directed from the trough of the sandwave towards the crest near the bed for both turbulence models (Figure 3). The numerical shallow water model adopted in this paper is capable in reproducing the tide averaged residual current as earlier found in the idealized model by Hulscher (1996).
Qualitatively, the circulation cells are similar for both turbulence models (Figure 3). However, compared to the constant eddy viscosity model, the k-ε turbulence model shows weaker near-bed velocities and the centre of the circulation cell is found closer the bed.

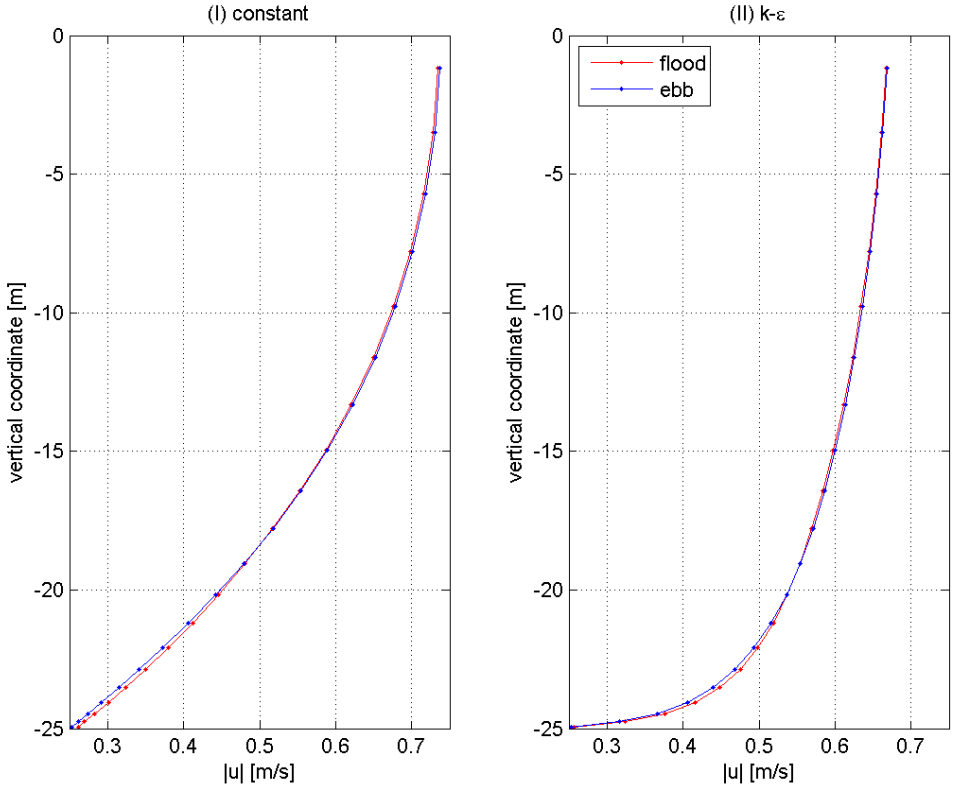

Figure 2. Absolute value of the maximum flow velocity during flood (red) and ebb (blue) for a simulation with the constant eddy viscosity model (left) and the k-ε turbulence model (right), halfway the slope of the central sandwave (x=-L/4) with a wavelength L = 600 m and an initial amplitude A_0 = 0.5 m.

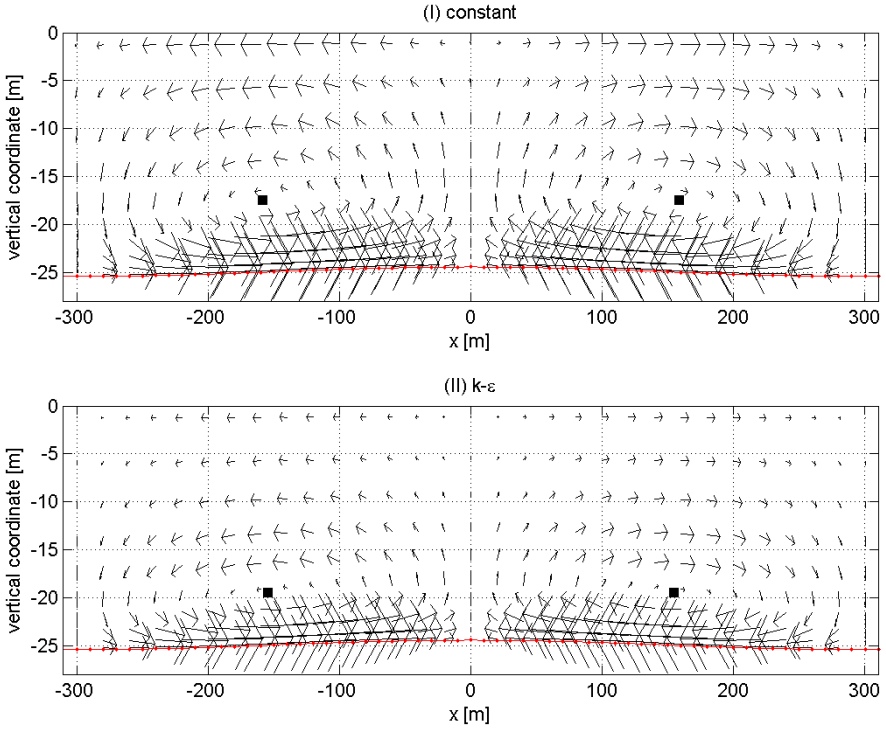

Figure 3. Tide averaged residual current, for a simulation with the constant vertical eddy viscosity model (upper panel) and the k-ε turbulence model (lower panel). The centre of the circulation cell is indicated with a black square. Wavelength L = 600 m and initial amplitude A_0 = 0.5 m.

3.2 Sediment transport and bed evolution

Now let us investigate the growth rate as a function of the topographic wave number $k = 2\pi/L$, for both turbulence models, and isolating the contributions due to the plain bed load (without bed slope) and the bed slope-induced transport. Assuming exponential growth (which is valid for small bed amplitudes), the growth rate γ_r for the bed perturbation is calculated by

$$\gamma_r = \frac{1}{T}\log\left(\frac{A_1}{A_0}\right), \qquad (10)$$

where T is the tidal period, A_1 is the bed amplitude of the sandwave at the end of the simulation and A_0 the initial bed amplitude. The amplitude of the sandwave after a single tidal cycle is determined by a Fast Fourier Transform (FFT) of the central part of the sandwave domain. Positive values of γ_r correspond to growth of the bottom perturbation, whereas negative values correspond to decay.

Given the direction of the tide averaged near bed velocities, a small net transport of sediment directed from the trough towards the crest of the sandwave is expected. For a given wavelength of the sandwave, water depth and flow velocity amplitude, the strength of the recirculation cell can be determined. In general, the sandwave with the largest wave number causes the strongest circulation cell. Consequently, the sandwave with the smallest wavelength shows the largest growth rate, for both turbulence models in case slope effects are not considered (Figure 4A). However, the growth rate for the constant eddy viscosity model is larger, due to the stronger tide averaged near bed velocities for a given wave number.

Due to the slope effect, the sandwave tends to decay. The slope effect is the strongest for large wave numbers, while this effect is a function of the slope of the bed form and the magnitude of the transport rate. The slope of the bed form is equal for both simulations for a given wave number, but the magnitude of the transport rate is much larger for the constant eddy viscosity model, resulting in a stronger slope effect (Figure 4B).

The total growth curve is the sum of both the plain bedload and the slope effect (Figure 4C). The fastest growing mode is the wave number which triggers the fastest initial growth. In conclusion, the wave number for the fastest growing mode for the constant eddy viscosity model is much smaller, compared to the k-ε turbulence model.

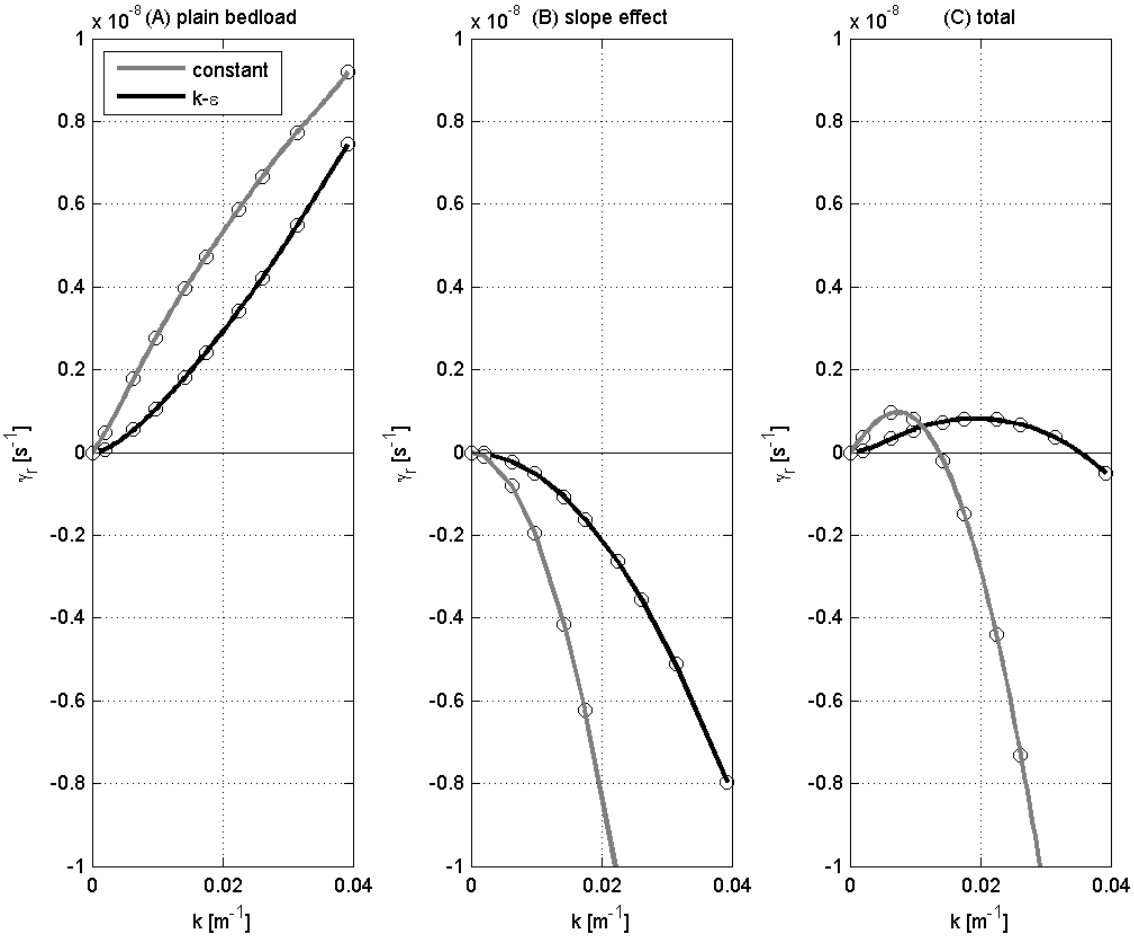

Figure 4. The total growth rate curve (C) is the summation of the bedload component (A) and the slope effect (B). On the x-axis the dimensionless wave number *k* is given on the y-axis the growth rate γ_r. Two turbulence models are shown: constant vertical eddy viscosity (gray) and k-ε turbulence closure model (black).

3.3 Comparison with observations from the North Sea

The results of the model are compared with field data on flow velocity amplitude, water depth, grain size and wavelength of sandwaves on the Dutch continental shelf (Van Santen et al., 2011). Because only bed load is included in the model, six locations are selected which are located in a water depth H_0 of around 30 meters, a flow velocity amplitude U of around 0.65 m/s and a grain size d of around 0.32 mm (Table 1), such that bed load is indeed expected to be the dominant transport mechanism.

Table 1. Wavelength L of sandwaves at six locations in the North Sea. Data on the amplitude of the flow velocity U, water depth H and grain size d are given by Van Santen et al. (2011).

Location no.	U (m/s)	H (m)	d (mm)	L (m)
'225'	0.70	21.33	0.36	220
'222'	0.73	34.63	0.34	490
'217'	0.68	29.30	0.27	290
'207'	0.72	31.51	0.28	320
'201'	0.64	25.70	0.36	400
'190'	0.65	30.59	0.32	290
range	[0.64 – 0.73]	[21.33 – 34.63]	[0.27 – 0.36]	[220 – 490]

The range in fastest growing mode is determined for both turbulence models by taking the mean of two of the three parameters and taking both the maximum and minimum of the third parameter (Table 1). The result of the simulation in which the k-ε turbulence model is used agrees much better with the field data compared to the constant eddy viscosity model (Figure 5).

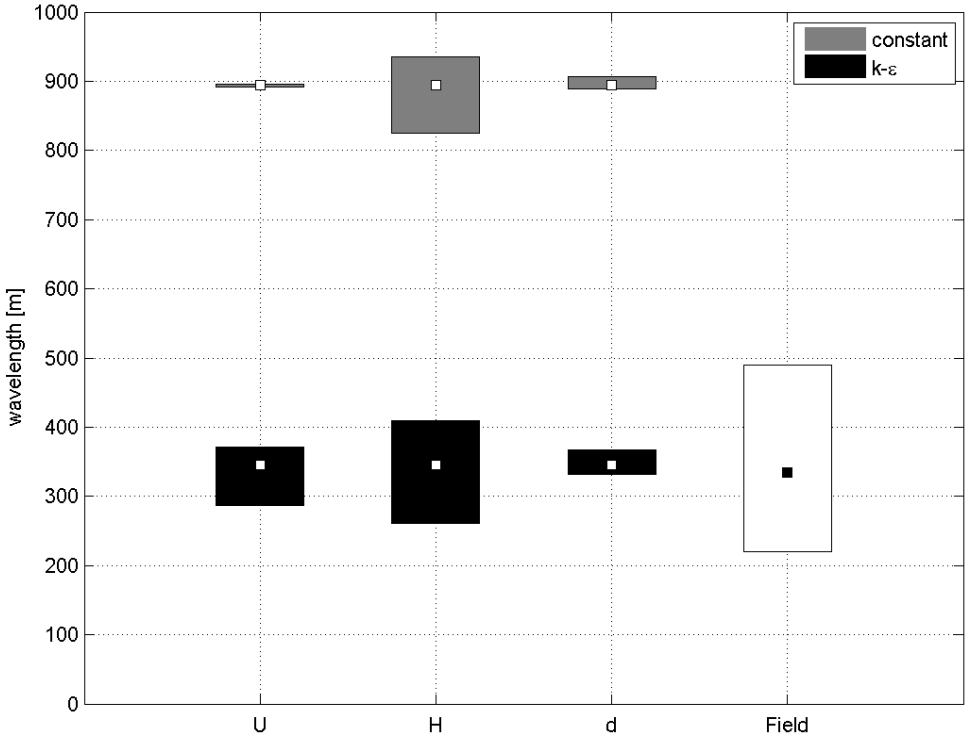

Figure 5. Range in fastest growing mode for the range in parameter settings given in Table 1, by varying the flow velocity amplitude U, mean water depth H_0 and grain size d while keeping the other parameters constant. Simulations with the constant eddy viscosity model are indicated with a gray bar, simulations with the k-ε turbulence model are indicated with a black bar, white bar indicates the variation in wavelength measured in the field, mean modeled wavelength is indicated with a white square and mean measured wavelength is indicated with a black square.

4 DISCUSSION

This paper presents simulations with the numerical shallow water model Delft3D in which sandwave formation has been reproduced. The formation of sandwaves has never been reproduced in a numerical shallow water model before. The main difficulty in reproducing sandwave formation in a numerical shallow water model is the reflection of the tidal wave by the imposed lateral boundary. In engineering practice, Delft3D is usually run with a flow velocity at one lateral boundary and a water level at the opposite lateral boundary. While these lateral boundary conditions are reflective, a small net tide averaged current will be present in the modeling domain. The magnitude of this reflective net current is in the same order of magnitude as the net current induced by the bottom topography (circulation cell: Figure 3). In this study, Riemann lateral boundary conditions have been used instead, in which outgoing waves can cross the open boundary without being reflected back into the computation domain.
The resolution used to reproduce sandwave formation is 10 m in horizontal direction in the sandwave domain and 20 layers in vertical direction, for which the layers close to the bed have a vertical resolution in the order of tens of centimeters. The fine horizontal resolution is necessary to have enough grid cells to cover the smallest sandwaves modeled (160 meter; Figure 4). The fine vertical resolution is necessary to model the strong gradient in flow velocity profile near the bed (Figure 3). Given the fine resolution in space and the need to model the complete tidal cycle in small time steps, given the time dependency of the vertical eddy viscosity, the total simulation time takes 30 minutes for the k-ε epsilon turbulence closure model. In contrast, the total simulation time for an idealized model takes less than 1 minute.
As shown in Section 3, the outcome of the numerical shallow water model is comparable to the outcome of the idealized models: sandwaves with a wavelength in the order of several hundreds of meters and a growth rate in the order of 0.01 year^{-1} are found. However, the shape of the growth curve is different near k=0 (Figure 4C). The growth curve for idealized models and the numerical model with constant eddy viscosity is concave, while the growth curve for the numerical model in which a k-ε turbulence model is adopted is convex.
The numerical shallow water model used in this paper offers the possibility to focus on the influence of suspended sediment transport on sandwave characteristics and the influence of a residual current and tide asymmetry on sandwave migration. Finally, the proposed model offers us the possibility to examine the saturation height of sandwaves.

5 CONCLUSIONS

Sandwave formation has been successfully reproduced in a numerical shallow water model (Delft3D). Special attention has been given to lateral boundaries which are non reflective and the high resolution needed both in time and space in order to resolve the residual current. The model has been run for two turbulence models: constant viscosity and k-ε. For the same physical forcing, the constant eddy viscosity model showed higher tide averaged near bed velocities, and consequently causing longer sandwaves compared to the k-ε turbulence model. Comparison of the model outcome with field data has been done by comparing field data on sandwave length of the southern North Sea with the results of both turbulence models. The k-ε turbulence model showed much better agreement with the field data. Future research should focus on the following three items: influence of suspended sediment transport on sandwave formation, influence of residual and tide asymmetry on sandwave migration and the saturation height of sandwaves.

6 ACKNOWLEDGEMENTS

This work is part of the PhD research of the first author, which is co-supported by the Dutch Technology Foundation STW, applied science division of NWO and the Technology Program of the Dutch Ministry of Economic Affairs. We thank Henk Schuttelaars, Bert Jagers and Fenneke Sterlini for useful discussions on this topic.

REFERENCES

Bagnold, R.A., 1956. the flow of cohesionless grains in fluids. Proc. Royal Soc. Philos. Trans., London, vol. 249, pp. 71-81.

Besio, G., Blondeaux, P., Brocchini, M., Vittori, G., 2004a. On the modelling of sand wave migration. Journal of Geophysical Research 109, 1–13.

Besio, G., Blondeaux, P., Vittori, G., 2006. On the formation of sand waves and sand banks. Journal of Fluid Mechanics 557, 1-27.

Borsje, B.W., De Vries, M.B., Bouma, T.J., Besio, G., Hulscher, S.J.M.H., Herman, P.M.J., 2009. Modelling bio-geomorphological influences for offshore sandwaves. Continental Shelf Research 29, 1289-1301.

Cherlet, J., Besio, G., Blondeaux, P. van Lancker, V., Verfaillie, E., Vittori, G., 2007. Modeling sand wave characteristics on the Belgian Continental Shelf and in the Calais-Dover Strait. Journal of Geophysical Research, Vol. 112, C06002, doi:10.1029/2007/JC004089.

Deltares, 2011. User manual Delft-3D FLOW, Deltares (www.deltares.nl), Delft, The Netherlands.

Dorst, L.L., Roos, P.C., Hulscher S.J.M.H., Lindenbergh, R.C., 2009. The estimation of sea floor dynamics from bathymetric surveys of a sand wave area. Journal of Applied Geodesy 3(3), 97-120.

Fredsøe, J., Deigaard, R., 1992. Mechanics of Coastal Sediment Transport. World Scientific.

Hulscher, S.J.M.H. 1996. Tidal-induced large-scale regular bed form patterns in a three-dimensional shallow water model. Journal of Geophysical Research C9, 101, 20727-20744.

Hulscher, S.J.M.H., Van den Brink, G.M. 2001. Comparison between predicted and observed sand waves and sand banks in the North Sea. Journal of Geophysical Research C5, 106, 9327-9338.

Knaapen, M.A.F., Hulscher, S.J.M.H., 2002. Regeneration of sand waves after dredging. Coastal Engineering 46, 277-289.

Lesser, G., Roelvink, J., van Kester, J., Stelling, G., 2004. Development and validation of a three-dimensional morphological model. Coastal Engineering 51, 883-915.

McCave, I.N., 1971. Sand waves in the North Sea off the coast of Holland. Marine Geology 10, 199-225.

Németh, A. A., Hulscher, S.J.M.H., De Vriend, H.J., 2003. Offshore sandwave dynamics, engineering problems and future solutions. Pipeline and Gas Journal 230, 67-69.

Németh, A.A., Hulscher, S.J.M.H., DeVriend, H.J., 2002. Modelling sand wave migration in shallow shelf seas. Continental Shelf Research 22, 2795–2806.

Németh, A. A., Hulscher, S.J.M.H., Van Damme, R.M.J., 2007. Modelling offshore sandwave evolution. Continental Shelf Research 27, 713-728.

Rodi, W., 1984. Examples of calculation methods for flow and mixing in stratified fluids. Journal of Geophysical Research 92, 5305-5328.

Sterlini, F.M., Hulscher, S.J.M.H., Hanes, D.M., 2009. Simulating and understanding sand wave variation: A case study of the Golden Gate sand waves. Journal of geophysical research 144(F02007).

Tonnon, P.K., van Rijn, L.C., Walstra, D.J.R., 2007. The morphodynamic modelling of tidal sand waves. Coastal Engineering 54, 279-296.

Van Dijk, T.A.G.P., Kleinhans, M.G., 2005. Processes controlling the dynamics of compound sand waves in the North Sea, Netherlands. Journal of Geophysical Reserach 110, 1-15.

Van Rijn, L. C., D. J. R. Walstra, and M. van Ormondt (2004), Description of TRANSPOR 2004 (TR2004) and implementation in DELFT3Donline, Rep. Z3748, Delft Hydraul., Delft, Netherlands.

Van Santen, R.B., de Swart, H.E., van Dijk, T.A.G.P., 2011. Sensitivity of tidal sand wavelength to environmental parameters: A combined data analysis and modeling approach. Continental Shelf Research 31, 966-978.

Verboom G.K., Slob, A., 1984. Weakly-reflective boundary conditions for two-dimensional water flow problems. Advances in water resources 7, 192-197.